ORIGINAL PAPER

Evolution trend of the Huangyanwo rock mass under the action of reservoir water fluctuation

Kaiqiang Zhang[1,2] · Luqi Wang[1] · Zhenwei Dai[3] · Bolin Huang[4] · Zhihua Zhang[1,2]

Abstract

The Huangyanwo rock mass (HRM) is distributed in the right bank cliffs of the Yangtze River. And the total volume of HRM is about 955,000 m^3, causing a large-scale rock mass at risk of failure. Herein, varieties of methods are used to investigate the development of cracks and broken regions in the high-steep area, underwater area, and internal areas of the HRM. Furthermore, the potential failure mechanism and the stability trend of HRM are proposed based on the detailed survey results and numerical simulation. To be specific, our study proves that the reservoir water could induce periodic mechanical state changes of HRM. When the water level rises, the deformation and shear stress of the HRM increase together with the decrease in stability and vice versa. Therefore, the stability of the HRM is likely to reach the critical state after 30 hydrological years considering the deterioration of broken areas under the action of reservoir water fluctuation. The relevant survey and analysis methods employed in this paper can provide valuable reference for the future evolution analysis of the reservoir bank.

Keywords On-site investigation · High-steep reservoir bank · Dry–wet cycles · Stability evaluation · Numerical simulation

List of symbols

σ	Axial compression
ε_x	The lateral strain
ε_y	The axial strain
θ	The porosity
θ_r	The residual water content
θ_s	The saturated water content
h	The matric potential

✉ Luqi Wang
wlq93@cqu.edu.cn

1 School of Civil Engineering, Chongqing University, Chongqing 400045, China

2 Chongqing 208 Geo-Environmental Research Institute Co. Ltd, Chongqing 400700, China

3 Central South China Innovation Center for Geosciences, Wuhan Centre of China Geological Survey, Wuhan 430205, Hubei, China

4 Hubei Key Laboratory of Disaster Prevention and Mitigation, China Three Gorges University, Yichang 443002, China

α, n and m	The empirical parameters of the water retention curve
γ	Unit weight
γ'	Saturated unit weight
E	Elastic modulus
μ	Poisson's ratio
C	Cohesion
φ	Friction angle
N	The number of dry–wet cycles

1 Introduction

Geological disasters in special geographical environment may cause extremely serious consequences (Budetta and De 2016; Fischer et al. 2012; Kumar et al. 2018; Wang et al. 2019a). For example, the Vajont landslide slipped into the reservoir area which caused more than 2,000 deaths (Crosta et al. 2016; Paronuzzi and Bolla 2015). And a landslide in Uttarakhand state of India in February 2021 damaged two hydropower plants, and more than 200 people were killed or missing (Shugar et al. 2021; Mao et al. 2022).

For the high-steep rocky bank, the periodic fluctuation of the reservoir water level is usually associated with the change of seepage filed and the deterioration of base rock mass (Yin et al. 2016, 2022; Wang et al. 2020a). This dynamic mechanical environment makes it challenging to determine the evolution trend (Hungr et al. 2014; Gu et al. 2021). The swell caused by the collapse of the rocky bank would further increase the difficulty of prevention and control (Yin et al. 2015). Therefore, it is particularly important to predict the critical instability state of high-steep rocky bank under complex mechanical environment (Huang et al. 2014, 2019). The big data-driven analytical methods (Xiao et al. 2021; Wang et al. 2020b, 2022; Yao et al. 2022), theoretical analysis (Huang et al. 2016; Yin et al. 2011; Yao et al. 2019), experimental investigation (Wang et al. 2020c; Zhu et al. 2020, 2022; Tao et al. 2021), and numerical simulation (Wang et al. 2020d, 2021a) are commonly used to analyze the evolution process of rocky bank. However, the detailed geo-mechanical data of rocky banks have always been the key to the validity of prediction methods, providing the basis for the accurate geo-mechanical models (Wang et al. 2020e, 2021b).

The Huangyanwo rock mass (HRM) is located at Three Gorges reservoir area, which is taken as a case to study. And a series of methods were employed to obtain the detailed geological information. The potential failure mechanism and the stability trend of the HRM under the action of reservoir water fluctuation were investigated by the laboratory tests and numerical simulation. The related methods developed in this paper can provide an important guidance for the evolution analysis of the high-steep reservoir bank.

2 Study area

The HRM is located in Peishi Township, Wushan County, Chongqing (N31°01′53″, E110°07′32″; Fig. 1). And it is distributed in the right steep bank of the Yangtze River. The slope of the cliff is about 80–90°. The stratums are mainly the residual slope sediments of Quaternary (Q_4^{el+dl}) and the Jialingjiang Formation of the Triassic (T_1j^{2-3}). There are primarily two sets of structural cracks with attitudes of 320–5°∠72–88° and 75–92°∠70–85°.
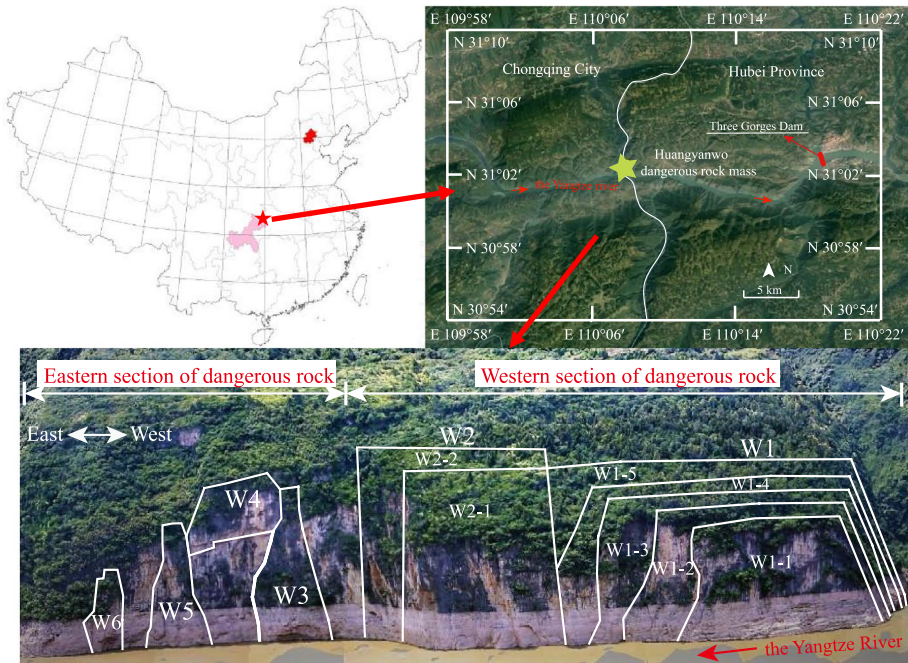
Fig. 1 An overview of the HRM

According to the formation characteristics, the HRM can be divided into east and west sections (Fig. 1). The length of the eastern section is 250 m, of which the deterioration zone (DZ; the elevation from 145 to 175 m) was eroded as rock cave under the action of dry–wet cycles. And western section of HRM is about 450 m, where the DZ is affected by unloading and water erosion, suffering dissolution, broken area, and weak structural plane problems. The unloading cracks on the top are outwardly inclined, and western section is divided from the bedrock with a block or plate shape.

The study area is located in a high and steep gorge, which is troubling to perform a detailed investigation by traditional methods. Therefore, a series of new methods were applied to study the formation and characteristics of HRM. Specifically, the single rope technique (SRT) and 3D oblique photography were used to investigate the high and steep areas of the HRM. Multi-beam sonar was used to determine the underwater areas of the HRM. A high-definition camera in a borehole, a wave velocity test, and cliff geophysical exploration were used to determine the development of cracks and broken areas inside the bank slope. The total volume of the HRM is about 955,000 m^3, which can be divided into six dangerous rock blocks. Among these blocks, the volume of the submerged dangerous rock monomer W1 is 540,000 m^3, which constitutes the main research object in this paper.

3 Formation characteristics of the HRM

Following the on-site investigation, four types of deformation characteristics were determined, including dissolution, unloading cracks, the hollowed out by water fluctuations, and the degradation of the base rock mass under dry–wet cycles.

Dissolution. The DZ in the study area is the limestone of the Jialingjiang Formation of the Triassic system (T_1j^3). It is a thin layered limestone from 145 to 170 m (Fig. 2). Influenced by water-level fluctuations, the dissolution degree of the limestone at this height interval is high, resulting in the formation of a weak broken area and concave rock cavity. The medium-thick layered limestone located above 170 m is relatively integrated (Fig. 2). An X-ray fluorescence spectrometer was used to analyze the rock minerals of the samples. The results showed that the mineral composition of the sample was mainly $CaCO_3$. Therefore, the development of the dissolution zone would be accelerated when exposed to water.

Unloading cracks. Due to the stress release and rock unloading, five cracks were formed at the top of the cliff, which are nearly parallel to the Yangtze River. The attitude of the unloading cracks is 354–3°∠83–88°, the length is 20–50 m, the width is 0.2–1.0 m, and the spacing is 1–5 m. The cracks extend from the top of the cliff to the river surface, and the upper part of the cracks is wider than that of the lower part. The characteristics of the unloading cracks at the top of the cliff were obtained using 3D oblique photography (Fig. 3).

Hollow-out by water-level fluctuations. Affected by the water fluctuations, the width of the cracks in the DZ is large, the dissolution pores are developed, and the local rock mass is broken (Fig. 4). Additionally, the broken rock mass in the DZ will be carried away by the water flow, causing local collapse.

Degradation of the base rock mass under dry–wet cycles. The base rock mass is a key area for the overall deformation and failure of the HRM. Since the base rock mass is near vertical and extends underwater, a series of new methods were applied to analyze the degradation of the base rock mass.
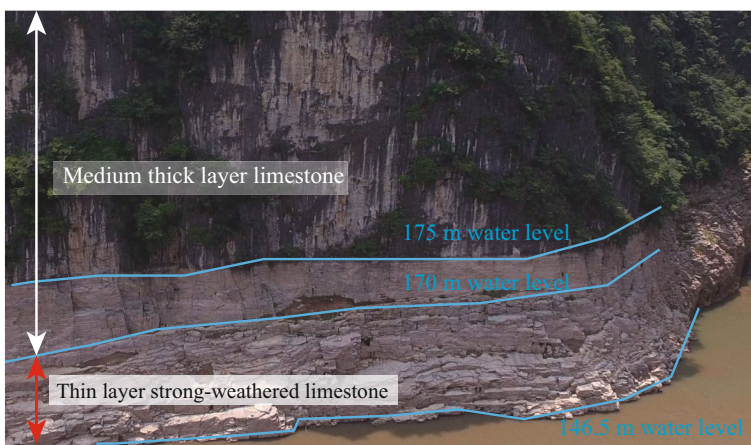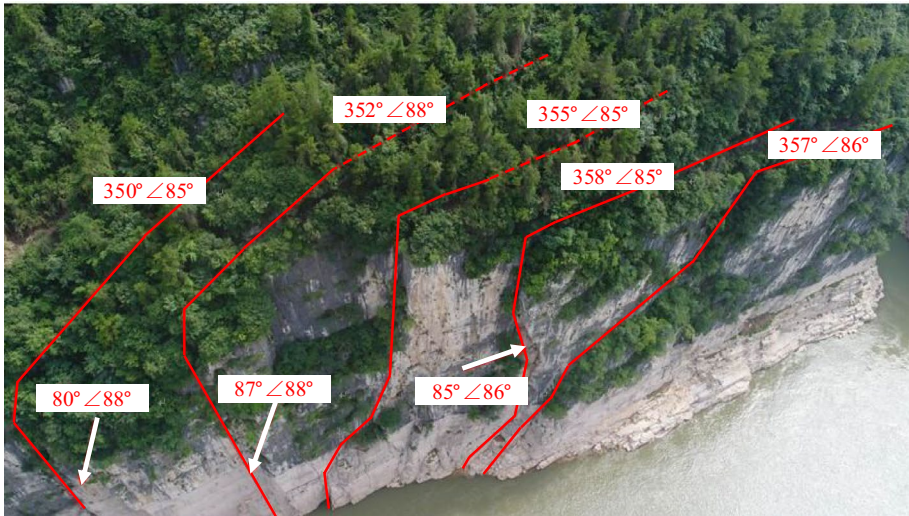

Fig. 2 Distribution of lithology

Fig. 3 Unloading crack at the top of the cliff (obtained using 3D oblique photography)

**Fig. 4** The broken area and dissolution cavity

(i) Survey mapping

The SRT and 3D oblique photography (Fig. 5a) were used to investigate the cracks and broken areas in the steep cliff. A total of 37 cracks were identified in the western section (Fig. 5b). According to the statistical analysis, the attitude of the cracks is 75–120°∠67–88° and the length is 20–110 m. It was determined that the crack was densely distributed in the DZ, and the development degree of the cracks in the DZ was higher than that of the upper zone.

(ii) High-definition camera technology and wave velocity test in the borehole
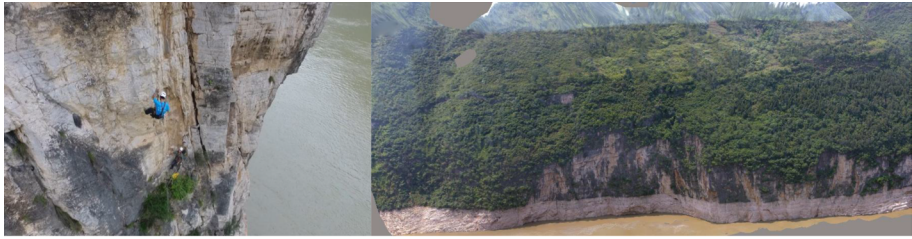
(a) SRT and 3D oblique photography
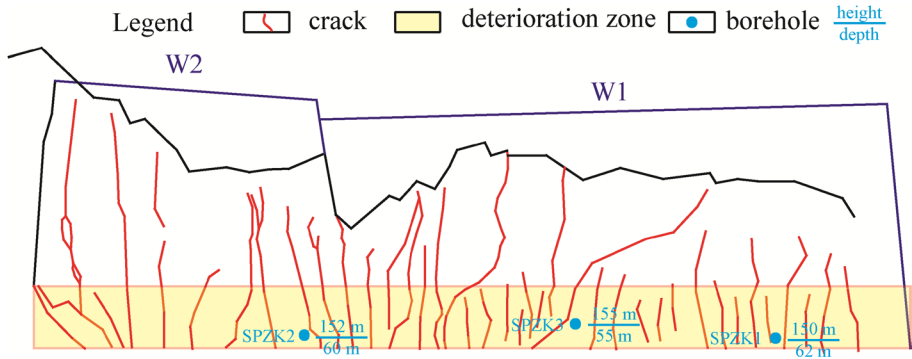
(b) The cracks in the submerged steep cliff

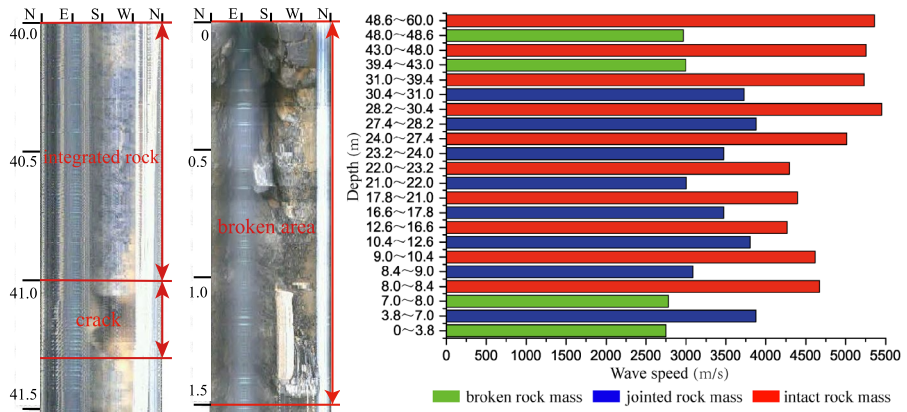**Fig. 5** The investigation of the submerged steep cliff

Fig. 6 The drilling results in the deterioration zone

A total of three horizontal drilling holes were placed in the DZ, and the drilling depth ranged from 55.0 to 62.0 m (Fig. 5b). After drilling, the internal geological conditions of the borehole were revealed using high-definition camera technology, and a wave velocity test was carried out in the borehole. SPZK1 was used as an example to interpret the results as follows (Fig. 6). Based on the imaging results
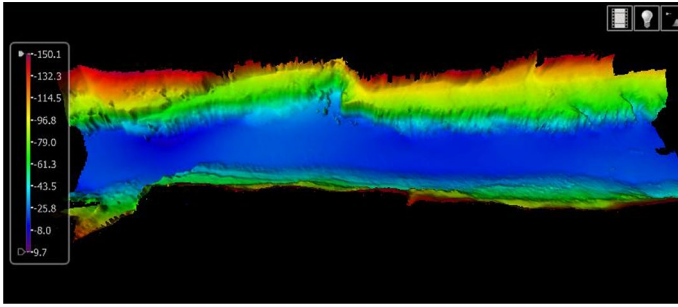
Fig. 7 Multi-beam sonar results

interpretation, significant cracks developed at 41.0–41.3 m. From 0 to 1.5 m, the rock mass is broken, the surface is rough, and the muddy composition is heavier, and thus it is identified as the broken area. The surface of the remaining section is smooth, which indicated that the rock mass is integrated. In addition, the rock mass integrity could also be identified according to the difference in wave velocity. For example, the sections of 0–3.8 m, 7.0–8.0 m, 39.4–43.0 m, and 48.0–48.6 m were characteristic of local broken or cracked rock masses.

(iii) The multi-beam sonar

The bottom elevation of the steep cliff is 85–110 m, which is below the minimum water level of 145 m in the Three Gorges reservoir area. A multi-beam sonar was first used to measure the underwater cliffs to more accurately detect the underwater cliff shape and the development of the concave rock cavity in the lower part of the HRM (Fig. 7).

(iv) The geophysical exploration on the cliff

In order to detect the development of broken areas and cracks inside the cliff, a geophysical exploration on the cliff was performed. The transient electromagnetic detection lines and geological radar test lines at 159 m elevation were arranged on the vertical cliff wall. According to the interpretation profile of the geological radar (Fig. 8a), a broken area and a dissolution zone were found at a height of 159 m. Additionally, in the area 5–20 m away from the cliff wall, the rock mass is broken. The results of the transient electromagnetic detection indicated that the resistivity of the DZ is abnormal, indicating that the rock mass is relatively broken (Fig. 8b). Based on all the above survey results, a comprehensive overview of the typical profile of W1 is shown in Fig. 8c.

4 Results

Based on the detailed investigation, it can be found that the formation and evolution process of the HRM are affected by geological factors, geological structural factors, and external dynamic factors.
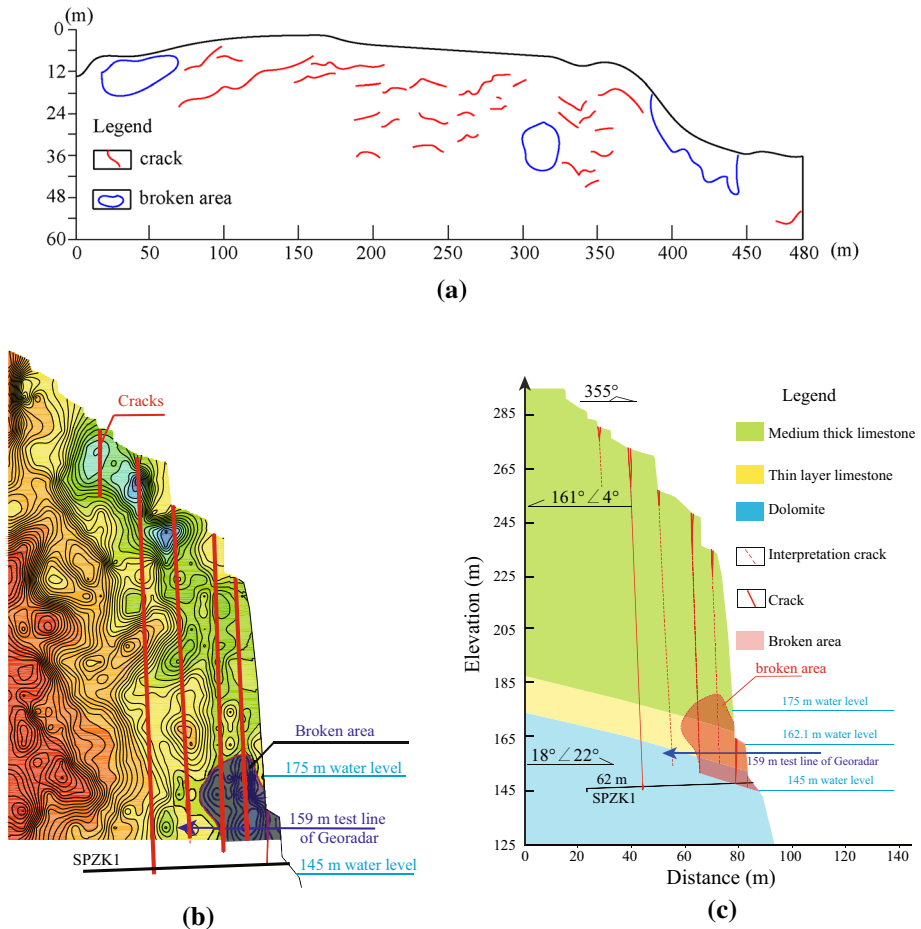
(i) Geological factors

Fig. 8 The geophysical exploration on the cliff. **a** The interpretation profile of geological radar. **b** Typical profile of the transient electromagnetic detection. **c** Comprehensive view of the typical profile of W1

The study area is located in a mountain gorge. The top elevation of the HRM is 220–280 m, the bottom elevation is 85–110 m, and the relative height difference is 135–170 m. The high-steep gorge geomorphology provides the necessary conditions for the formation of a dangerous rock. The upper part of the HRM (with an elevation above 170 m) is mainly medium-thick layered limestone, which has high strength. The lower part in the deterioration zone ranges from 145 to 170 m in elevation and mainly constitutes thin-layered limestone with corrosion cracks and cavity pores. This part of the rock mass is block-shaped, and the unloading cracks are externally inclined. Shear outlet areas can be formed easily under these conditions.

(ii) Geological structural factors

The HRM is located at the end of the south wing of the Guandu syncline, and the secondary structure is developed along the riverside. The rock formation in the upper middle part of the cliff is gentle; the dip angle of the stratum is about 4–20°; the stratum attitude of the western part of the HRM is 18–25°∠3–22°; and the stratum

attitude of the eastern part of the HRM is 127–160°∠3–20°. The formation of HRM is mainly controlled by two sets of dominant cracks. The cracks at the top of the cliff are parallel to the Yangtze River with an attitude of 320–5°∠72–88°. The other set of cracks is perpendicular to the steep cliff wall with an attitude of 75–92°∠70–85°. The boundaries of the HRM are formed by these two sets of tectonic cracks in the study area. Under the trigger of external factors, the HRM would collapse.

(iii)   Trigger factors for collapse

Fluctuations in reservoir water level. The base of the HRM is located in the DZ, which was formed by periodic water-level fluctuations from 145 to 175 m in the Three Gorges reservoir area. The base rock mass has deteriorated under the influence of the long-term water-level fluctuations. Concurrently, due to long-term erosion and abrasion, the broken area has become weakened and disintegrated, thus promoting the deformation and failure of the HRM. Due to the large volume of the HRM, the broken area or the weak structural plane of the steep cliff has been deformed under the action of gravity. Furthermore, the concentration of the stress in the broken area would intensify the deterioration degree of the base rock mass. This constitutes a key factor in the instability of HRM.

Rainfall. After precipitation, the surface water leaks along the trailing edge cracks into the rock mass, which reduces the mechanical properties of the cracks, increases the water pressure inside the cracks, and promotes the collapse of the HRM.

Root wedging of plants. The vegetation in the study area is flourishing, and the roots and stems of the plants have grown along the rock layers and cracks. The root wedging would expand the cracks and accelerate the deformation in the direction of the free face.

Action of thermal difference. The temperature difference between day and night or seasons in the study area is large. The thermal expansion and contraction due to the temperature changes would reduce the strength of the rock mass, thereby causing the weathering damage of the rock mass.

4.1 Failure mode

The broken areas of the base rock mass are affected by reservoir water fluctuations. Under the action of dry–wet cycles, the strength of the rock mass gradually reduces, and the broken area expands. Furthermore, the dissolution zone is gradually softened and the bond strength of the structural plane is reduced, resulting in the stress being concentrated in the broken area. The broken area is continuously pressed and sheared under the long-term high stress caused by the self-weight of the HRM.

Since the impoundment of the Three Gorges reservoir area in 2008, the dry–wet cycles continuously weaken the broken area in the DZ, accelerating the failure of the HRM.

4.2 The mechanical state of the typical profile in a single hydrological year

Based on the on-site investigation and failure mechanism analysis, the mechanical states and the factor of safety (FOS) in a single hydrological year are analyzed. The simulation through c-φ reduction algorithm by finite elements is adapted by the Midas software. When the slope reaches instability, the numerical non-convergence occurs simultaneously. The FOS is then obtained by c-φ reduction algorithm. The meshing density of the water-side area was higher than that of the trailing edge. Totally, 6169 meshes were divided, shown in Fig. 9. The element meshes are mainly quadrilateral, and there are only few

Fig. 9 The numerical model of HDM

175 m water level

Periodic transition

145 m water level
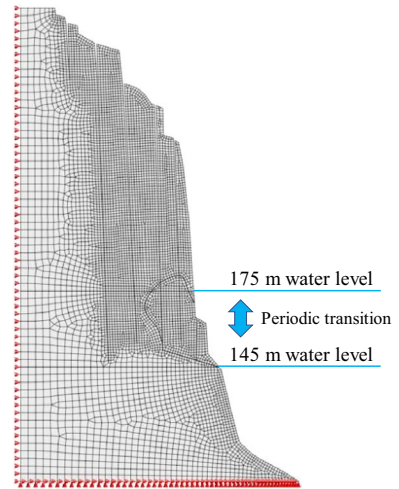
triangular elements used to ensure the mesh uniformity. Specifically, the leading and trailing edges are meshed with 1 m and 2 m as the basic unit, respectively. Meanwhile, the mesh division from the leading edge to the trailing edge adopts the method of size gradient to ensure the uniformity of mesh distribution. Before the iterative calculation, the element meshes of the leading edge were checked and the convergence of meshes can be guaranteed. That is, under the existing meshing method used in this paper, the real-time mechanical state can be effectively presented. The related meshing methods are built into the analysis process and widely adopted (Wang et al. 2019b, 2020d). The left boundary is constrained by the horizontal displacement, and the bottom boundary is constrained by the two-direction displacement. Furthermore, the monitored reservoir water level is applied to the right boundary to establish the transient seepage field. The Mohr–Coulomb model is selected for the numerical calculation. Notably, this paper focuses on the evolution process of the rocky bank under the action of reservoir water fluctuation. The results obtained by the Mohr–Coulomb model can further highlight the related trends, and the parameters involved in the Mohr–Coulomb model are easier to be obtained through laboratory experiments (Table 1). Especially when the strength reduction method based on the finite element is used to evaluate the stability of the slope, the Mohr–Coulomb model could connect with traditional evaluation methods such as the limit equilibrium method (Wang et al. 2020e).

In this paper, the vG function is used to perform the seepage calculation and describe the water retention curve of fractured rock (Ghanbarian-Alavijeh et al. 2010):

Table 1 The parameters used in numerical calculations

Lithology	Unit weight γ (kN/m^3)	Saturated unit weight γ' (kN/m^3)	Elastic modulus E (MPa)	Poisson's ratio μ	Cohesion c (MPa)	Friction angle φ (°)
The broken area	26.82	26.91	4268	0.30	0.628	42.57
The bedrock			47,800	0.20	5.210	44.40
Lithology	Porosity θ	θ_r	θ_s	α	n	m
The broken area	0.10	0.35	0.64	0.2	3	0.7

$$\frac{\theta - \theta_r}{\theta_s - \theta_r} = \frac{1}{\left[1 + (\alpha h)^n\right]^m} \tag{1}$$

where θ_r is the residual water content, θ_s is the saturated water content, h is the matric potential (kPa); α (kPa^{-1}), and n and m ($m = 1 - 1/n$) are empirical parameters. In the calculation process, the unsaturated seepage process of the rock mass is simplified in order to obtain a qualitative analysis. In addition to the difference in initial porosity between the broken area and the bedrock, other seepage parameters are set the same. The rocks taken from the study area were processed into standard cylindrical specimens with a diameter of 50 mm and a height of 100 mm. The stress–strain curves ($\sigma-\varepsilon$) of the rock can be obtained by uniaxial compression test, involving the axial strain ε_y and lateral strain ε_x. The elastic modulus is the average slope of straight-line segments of $\sigma-\varepsilon_y$ curve. And the Poisson's ratio is the value of axial strain to lateral strain, that is $\varepsilon_x/\varepsilon_y$. The triaxial compression tests are carried out under different confining pressures, and multiple Mohr's circles are drawn to obtain the shear strength curve of the rock. Then, according to the intercept of the line on the longitudinal axis and the angle between the line and the horizontal line, the cohesion and friction angle of the rock can be obtained (Ulusay 2014). The parameters used in numerical calculations are shown in Table 1.

In a single hydrological year, three mechanical states are selected for analysis, involving the water level of 175 m (the highest reservoir water level), the water level of 145 m (the lowest reservoir water level), and the water level of 162 m (reservoir water level under a 50-year torrential rain). Furthermore, the 162 m water level can be divided into two types: rising water level and falling water level.

The pore water pressure distributions under different water levels are shown in Fig. 10. Under the water level of 175 m, the pore water pressure is the largest, reaching 735.49 kPa; under the water level of 145 m, the pore water pressure is the smallest (442.08 kPa). At the water level of 162 m, the maximum pore water pressure when the water level rises (612.72 kPa) is slightly greater than that (608.60 kPa) when the water level drops.

The deformation distribution under different water levels (Fig. 11) indicated that the maximum deformation area is concentrated at the divided blocks underlying the broken area. At the water level of 175 m, the deformation is the largest, up to 0.2409 m; at the water level of 145 m, the deformation is the smallest (0.2255 m). At the water level of 162 m, the maximum deformation when the water level rises (0.2269 m) is slightly greater than that (0.2266 m) when the water level drops.

The shear stress distribution indicated that the shear stress is distributed at the trailing cracks in of each divided block (Fig. 12). At the water level of 175 m, the max shear stress is the largest, reaching 7.823 MPa; at the water level of 145 m, the max shear stress is the smallest (7.323 MPa). At the water level of 162 m, the maximum shear stress when the water level rises (7.368 MPa) is slightly larger than that (7.359 MPa) when the water level drops.

The plastic strain distribution indicated that the plastic strain is concentrated in the tip area of the second submerged crack (Fig. 13). At the water level of 175 m, the max plastic strain is the largest, reaching 0.06327; at the water level of 145 m, the max plastic strain is the smallest (0.05922); the max plastic strain (0.05958) at the rising water level of 162 m is greater than that (0.05951) at the falling water level of 162 m. Furthermore, when the reservoir water level is the highest (175 m), the stability is the lowest; when the reservoir water level is the lowest (145 m), the stability is the highest; the stability of the falling water level is higher than that of the rising water level.
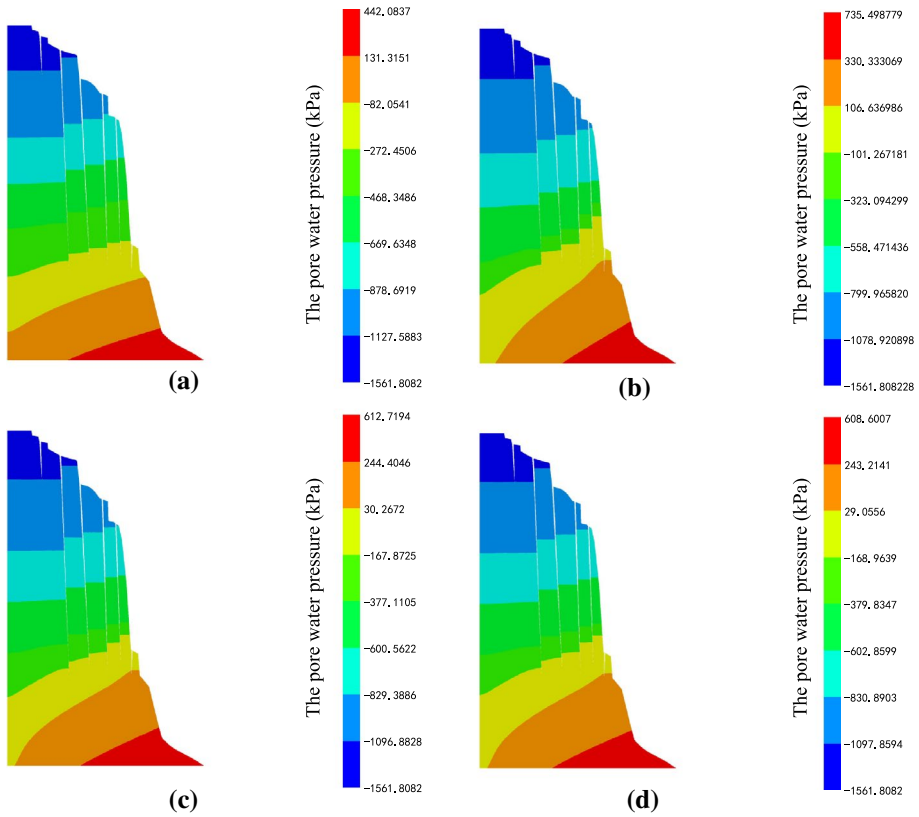
Fig. 10 The pore water pressure distribution under different water levels. **a** The water level of 145 m. **b** The water level of 175 m. **c** The rising water level of 162 m. **d** The falling water level of 162 m

5 Discussion

The evolution trend depends on the periodic rise and fall of the reservoir water level. To further predict the mechanical state as the number of hydrological years increases, the deterioration of the broken area under the dry–wet cycles was considered. The related mechanical parameters are provided by the Chongqing 208 Geological Team (Table 2). Notably, the rocks have different sensitivities to dry–wet cycles (Hu et al. 2020; Gu et al. 2021; Xu et al. 2021), and the mechanical properties listed in Table 2 could be decrease in a certain range of dry–wet cycles.

Through the coupling calculation of rock mass degradation and water-level fluctuation, the maximum deformation, maximum shear stress, and FOS can be obtained (Fig. 14). A total of 36 hydrological years have been calculated from the initial state to the instability. It can be found that the mechanical state changes with the rise and fall of the water level. When the water level rises, the deformation and shear stress increase, and the FOS decreases; when the water level drops, the deformation and shear stress decrease, and the
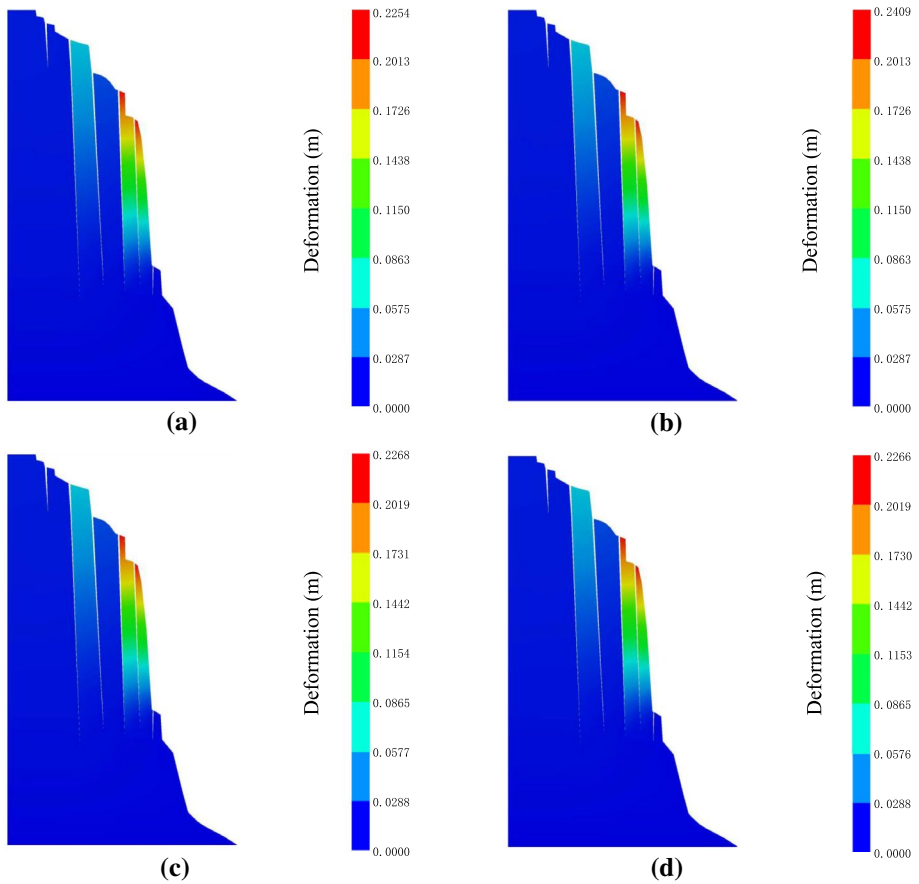
Fig. 11 The deformation distribution under different water levels. **a** The water level of 145 m. **b** The water level of 175 m. **c** The rising water level of 162 m. **d** The falling water level of 162 m

FOS increases. Moreover, the FOS is the lowest and the deformation is the largest at the water level of 175 m. Correspondingly, when the water level reaches 145 m, the stability is the highest and the deformation is the smallest.

With the increase in the number of water-level fluctuations, the deformation and shear stress gradually increase, and the stability gradually decreases. In the 30th hydrological year, the stability reached a critical state at the water level of 175 m (the lowest stability in a single hydrological year). After 36 hydrological years, the HRM become instable at the water level of 145 m (the highest stability in a single hydrological year).

In this paper, the deterioration of broken area under the action of reservoir water fluctuation was determined as the key factor to the failure mechanism. After identifying the gradual evolution process, it is also important to control the potential risk caused by the dynamic collapse, which will be further investigated in subsequent research.
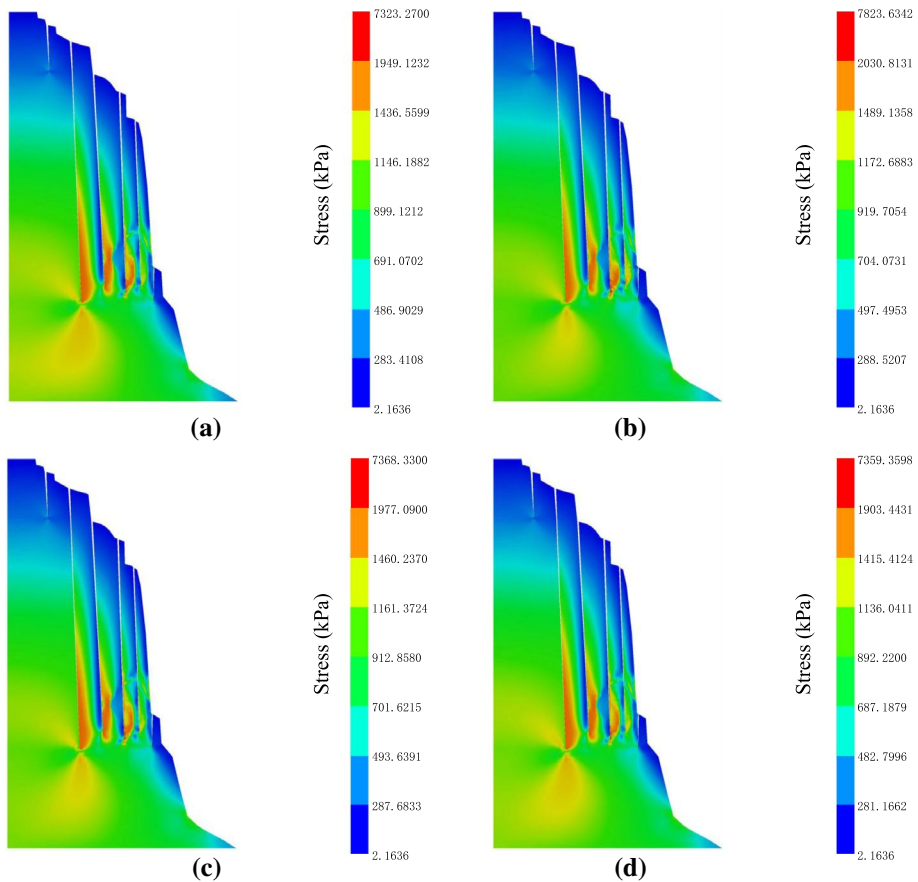
Fig. 12 The shear stress distribution under different water levels. **a** The water level of 145 m. **b** The water level of 175 m. **c** The rising water level of 162 m. **d** The falling water level of 162 m

6 Conclusions

Based on the on-site investigation using a series of methods, the development of cracks and broken areas of the HRM was studied in detail. Furthermore, the formation and failure mechanisms of the HRM were revealed through the numerical calculation of hydraulic coupling.

It can be found that the change of pore water pressure caused by the reservoir water can further induce periodic changes in the mechanical state of the reservoir banks. When the water level reaches 175 m, the stability is the lowest and the deformation is the largest. When the water level reaches 145 m, the stability is the highest and the deformation is the smallest. Under the same water level, the stability is higher than that when the water level drops. The corresponding relationship between the mechanical state and the fluctuation of the water level in different hydrological years is basically the same.

After considering the deterioration of broken area under the action of reservoir water fluctuation, the stability would reach the critical state after 30 hydrological years. As the
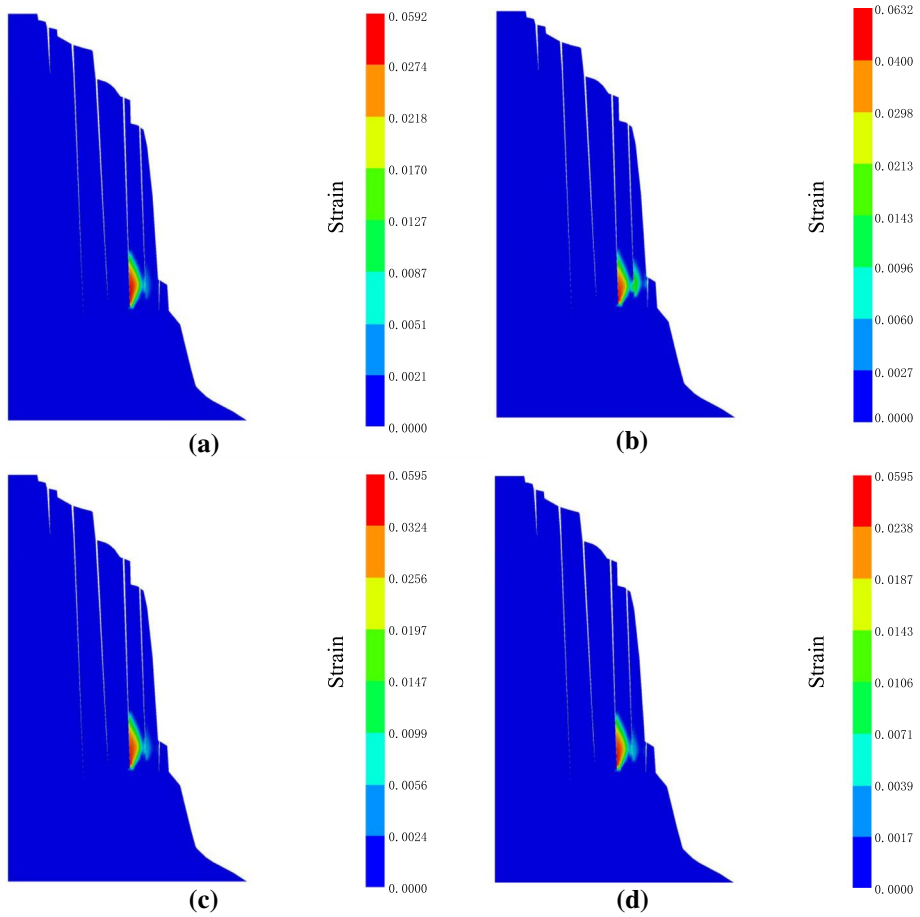
Fig. 13 The plastic strain distribution under different water levels. **a** The water level of 145 m (FOS = 1.40). **b** The water level of 175 m (FOS = 1.31). **c** The rising water level of 162 m (FOS = 1.38). **d** The falling water level of 162 m (FOS = 1.39)

Table 2 The deteriorated mechanical parameters of the broken area

Mechanical parameters	Unit	The N dry–wet cycle ($0 \leq N \leq 50$)
Elastic modulus E	MPa	$-59N + 4268$
Cohesion c	kPa	$-6.0875N + 682.13$
Friction angle φ	°	$-0.2252N + 42.57$

number of water-level fluctuations increases, the damage degree and deformation of the broken area would increase, and the management will become increasingly difficult. Therefore, it is recommended to perform the treatment as soon as possible while monitoring on-site.
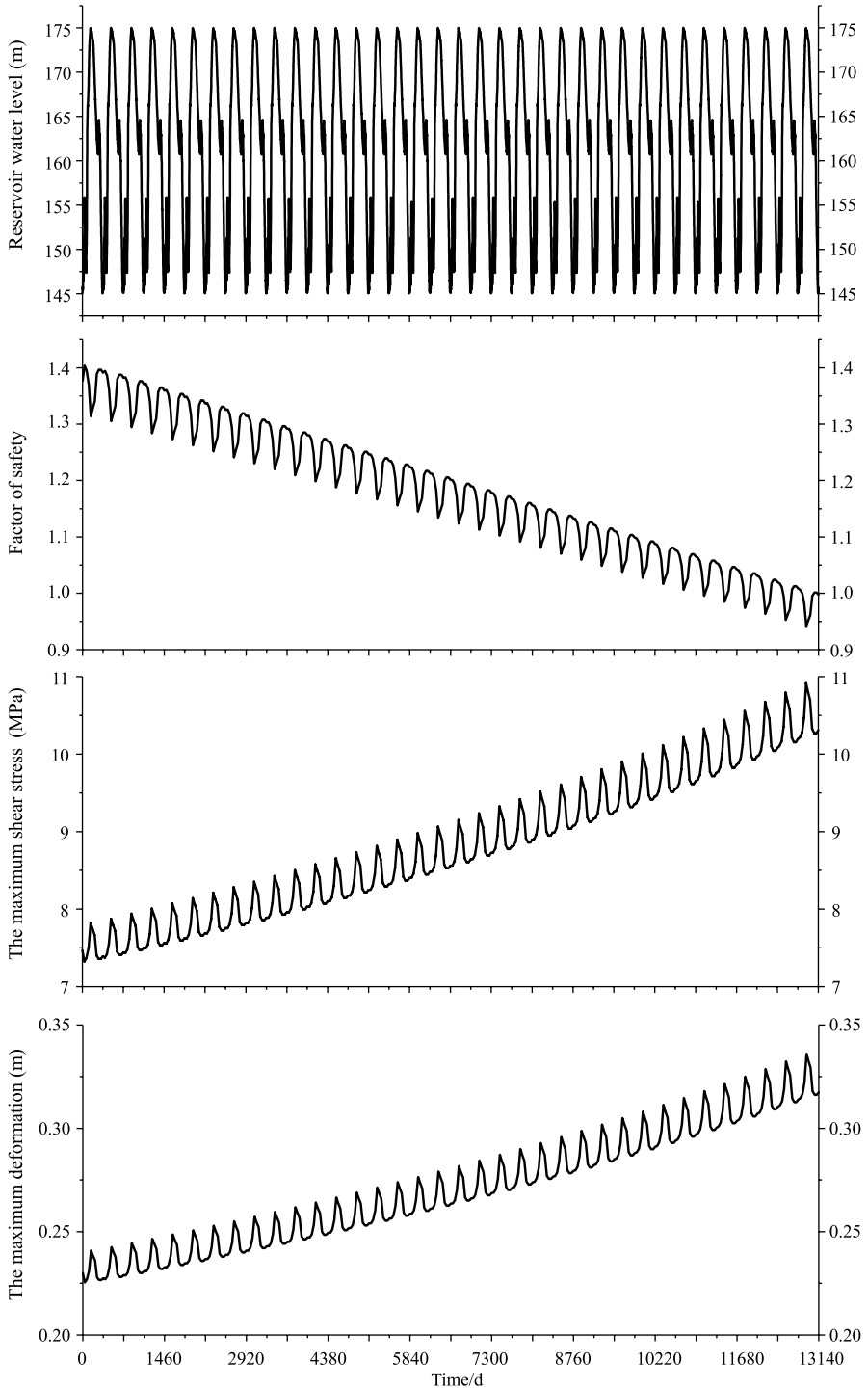
Fig. 14 Evolution curves of the HRM in multiple hydrological years

Declarations

Conflict of interest We declare that we have no financial and personal relationships with other people or organizations that can inappropriately influence our work, and there is no professional or other personal interest of any nature or kind in any product, service, and/or company that could be construed as influencing the position presented in, or the review of, the manuscript entitled, "Evolution trend of the Huangyanwo rock mass under the action of reservoir water fluctuation."

References

Budetta P, De LC (2016) Wedge failure hazard assessment by means of a probabilistic approach for an unstable sea-cliff. Nat Hazards 76(2):1219–1239

Crosta GB, Imposimato S, Roddeman D (2016) Landslide spreading, impulse water waves and modelling of the vajont rockslide. Rock Mech Rock Eng 49(6):2413–2436

Fischer L, Purves RS, Huggel C, Noetzli J, Haeberli W (2012) On the influence of topographic, geological and cryospheric factors on rock avalanches and rockfalls in high-mountain areas. Nat Hazard 12:241–254

Ghanbarian-Alavijeh B, Liaghat A, Huang GH, Van Genuchten MT (2010) Estimation of the van Genuchten soil water retention properties from soil textural data. Pedosphere 20(4):456–465

Gu DM, Liu HL, Gao XC, Huang D, Zhang WG (2021) Influence of cyclic wetting-drying on the shear strength of limestone with a soft interlayer. Rock Mech Rock Eng 54(8):4369–4378

Hu CM, Yuan YL, Mei Y, Wang XY, Liu Z (2020) Comprehensive strength deterioration model of compacted loess exposed to drying-wetting cycles. Bull Eng Geol Environ 79(1):383–398

Huang BL, Yin YP, Wang SC, Chen XT, Liu GL, Jiang ZB, Liu JZ (2014) A physical similarity model of an impulsive wave generated by Gongjiafang landslide in Three Gorges Reservoir, China. Landslides 11(3):513–525

Huang BL, Zhang ZH, Yin YP, Ma F (2016) A case study of pillar-shaped rock mass failure in the Three Gorges Reservoir Area, China. Q J Eng GeolHydrogeol 49(3):195–202

Huang BL, Yin YP, Tan JM (2019) Risk assessment for landslide-induced impulse waves in the Three Gorges Reservoir, China. Landslides 16(3):585–596

Hungr O, Leroueil S, Picarelli L (2014) The Varnes classification of landslide types, an update. Landslides 11(2):167–194

Kumar V, Gupta V, Jamir I (2018) Hazard evaluation of progressive Pawari landslide zone, Satluj valley, Himachal Pradesh, India. Nat Hazards 93(2):1029–1047

Mao WF, Wu LX, Singh RP, Qi Y, Xie BS, Liu YJ, Ding YF, Zhou ZL, Li J (2022) Progressive destabilization and triggering mechanism analysis using multiple data for Chamoli rockslide in 7 February 2021. Geomat Nat Hazards Risk 13(1):35–53

Paronuzzi P, Bolla A (2015) Gravity-induced rock mass damage related to large en masse rockslides: evidence from Vajont. Geomorphology 234:28–53

Shugar DH, Jacquemart M, Shean D, Bhushan S, Upadhyay K, Sattar A, Schwanghart W et al (2021) A massive rock and ice avalanche caused the 2021 disaster at Chamoli, Indian Himalaya. Science 373(6552):300–306

Tao ZG, Zhu C, He MC, Karakus M (2021) A physical modeling-based study on the control mechanisms of negative poisson's ratio anchor cable on the stratified toppling deformation of anti-inclined slopes. Int J Rock Mech Min Sci 138:104632

Ulusay R (2014) The Isrm suggested methods for rock characterization, testing and monitoring: 2007–2014. Springer, Cham

Wang LQ, Yin YP, Huang BL, Zhang ZH, Wei YJ (2019a) Formation and characteristics of Guang'an Village landslide in Wuxi, Chongqing, China. Landslides 16(1):127–138

Wang LQ, Yin YP, Zhang ZH, Huang BL, Wei YJ, Zhao P, Hu MJ (2019b) Stability analysis of the Xinlu Village landslide (Chongqing, China) and the influence of rainfall. Landslides 16:1993–2004

Wang LQ, Yin YP, Huang BL, Dai ZW (2020a) Damage evolution and stability analysis of the Jianchuandong dangerous rock mass in the Three Gorges Reservoir Area. Eng Geol 265:105439

Wang YK, Huang JS, Tang HM, Zeng C (2020b) Bayesian back analysis of landslides considering slip surface uncertainty. Landslides 17(9):2125–2136

Wang LQ, Yin YP, Zhou CY, Huang BL, Wang WP (2020c) Damage evolution of hydraulically coupled Jianchuandong dangerous rock mass. Landslides 17:1083–1090

Wang LQ, Huang BL, Zhang ZH, Dai ZW, Zhao P (2020d) Hu MJ (2020d) The analysis of slippage failure of the HuangNanBei slope under dry-wet cycles in the Three Gorges Reservoir Region, China. Geomat Nat Hazards Risk 11(1):1233–1249

Wang LQ, Yin YP, Huang BL, Zhang ZH, Zhao P, Wei YJ (2020e) A study of the treatment of a dangerous thick submerged rock mass in the three gorges reservoir area. Bull Eng Geol Environ 79(5):2579–2590

Wang LQ, Wu JH, Zhang WG, Wang L, Cui W (2021a) Efficient seismic stability analysis of embankment slopes subjected to water level changes using gradient boosting algorithms. Front Earth Sci 9:807317

Wang LQ, Zhang ZH, Huang BL, Hu MJ, Zhang CY (2021b) Triggering mechanism and possible evolution process of the ancient Qingshi landslide in the Three Gorges Reservoir. Geomat Nat Hazards Risk 12(1):3160–3174

Wang YK, Tang HM, Huang JS, Wen T, Ma JW, Zhang JR (2022) A comparative study of different machine learning methods for reservoir landslide displacement prediction. Eng Geol 298:106544

Xiao T, Yu LB, Tian WM, Zhou C, Wang LQ (2021) Reducing local correlations among causal factor classifications as a strategy to improve landslide susceptibility mapping. Front Earth Sci 9:781674

Xu JB, Sun HH, Cui YL, Fei DY, Lan HX, Yan CG, Bao H, Wu FQ (2021) Study on dynamic characteristics of diorite under dry-wet cycle. Rock Mech Rock Eng 54(12):6339–6349

Yao WM, Li CD, Zuo QJ, Zhan HB, Criss RE (2019) Spatiotemporal deformation characteristics and triggering factors of Baijiabao landslide in Three Gorges Reservoir region, China. Geomorphology 343:34–47

Yao WM, Li CD, Yan CB, Zhan HB (2022) Slope reliability analysis through Bayesian sequential updating integrating limited data from multiple estimation methods. Landslides. https://doi.org/10.1007/s10346-021-01812-4

Yin YP, Sun P, Zhu JL, Yang SY (2011) Research on catastrophic rock avalanche at Guanling, Guizhou, China. Landslides 8(4):517–525

Yin YP, Huang BL, Liu GN, Wang SC (2015) Potential risk analysis on a Jianchuandong dangerous rockmass-generated impulse wave in the Three Gorges Reservoir, China. Environ Earth Sci 74(3):2595–2607

Yin YP, Huang BL, Wang WP, Wei YJ, Ma XH, Ma F, Zhao CJ (2016) Reservoir-induced landslides and risk control in Three Gorges Project on Yangtze River, China. J Rock Mech Geotech Eng 8(5):577–595

Yin YP, Wang LQ, Zhang WG, Dai ZW (2022) Research on the collapse process of a thick-layer dangerous rock on the reservoir bank. Bull Eng Geol Env. https://doi.org/10.1007/s10064-022-02618-x

Zhu C, He MC, Karakus M, Cui XB, Tao ZG (2020) Investigating toppling failure mechanism of anti-dip layered slope due to excavation by physical modelling. Rock Mech Rock Eng 53(11):5029–5050

Zhu C, Karakus M, He MC, Meng QX, Shang JL, Wang Y, Yin Q (2022) Volumetric deformation and damage evolution of Tibet interbedded skarn under multistage constant-amplitude-cyclic loading. Int J Rock Mech Min Sci 152:105066